



HAL
open science

From Substrate to Fragments to Inhibitor Active In Vivo against *Staphylococcus aureus*

Muriel Gelin, Julie Paoletti, Marie-Anne Nahori, Valérie Huteau, Clarisse Leseigneur, Grégory Jouvion, Laurence Dugué, David Clément, Jean-Luc Pons, Liliane Assairi, et al.

► To cite this version:

Muriel Gelin, Julie Paoletti, Marie-Anne Nahori, Valérie Huteau, Clarisse Leseigneur, et al.. From Substrate to Fragments to Inhibitor Active In Vivo against *Staphylococcus aureus*. *ACS Infectious Diseases*, 2020, 6 (3), 10.1021/acsinfecdis.9b00368 . hal-02573173

HAL Id: hal-02573173

<https://hal.science/hal-02573173>

Submitted on 29 May 2020

HAL is a multi-disciplinary open access archive for the deposit and dissemination of scientific research documents, whether they are published or not. The documents may come from teaching and research institutions in France or abroad, or from public or private research centers.

L'archive ouverte pluridisciplinaire **HAL**, est destinée au dépôt et à la diffusion de documents scientifiques de niveau recherche, publiés ou non, émanant des établissements d'enseignement et de recherche français ou étrangers, des laboratoires publics ou privés.



Distributed under a Creative Commons Attribution - NonCommercial 4.0 International License

From Substrate to Fragments to Inhibitor Active *In Vivo* against *Staphylococcus aureus*

Muriel Gelin,[¶] Julie Paoletti,[¶] Marie-Anne Nahori,[¶] Valérie Huteau,[¶] Clarisse Leseigneur,[¶] Grégory Jouvion, Laurence Dugué, David Clément, Jean-Luc Pons, Liliane Assairi, Sylvie Pochet,^{*} Gilles Labesse,^{*} and Olivier Dussurget^{*}



Cite This: <https://dx.doi.org/10.1021/acscinfecdis.9b00368>



Read Online

ACCESS |



Metrics & More



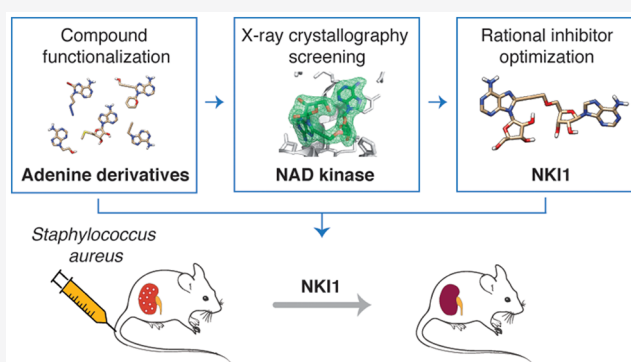
Article Recommendations



Supporting Information

ABSTRACT: Antibiotic resistance is a worldwide threat due to the decreasing supply of new antimicrobials. Novel targets and innovative strategies are urgently needed to generate pathbreaking drug compounds. NAD kinase (NADK) is essential for growth in most bacteria, as it supports critical metabolic pathways. Here, we report the discovery of a new class of antibacterials that targets bacterial NADK. We generated a series of small synthetic adenine derivatives to screen those harboring promising substituents in order to guide efficient fragment linking. This led to NKI1, a new lead compound inhibiting NADK that showed *in vitro* bactericidal activity against *Staphylococcus aureus*. In a murine model of infection, NKI1 restricted survival of the bacteria, including methicillin-resistant *S. aureus*. Collectively, these findings identify bacterial NADK as a potential drug target and NKI1 as a lead compound in the treatment of staphylococcal infections.

KEYWORDS: adenosine derivative, bacterial NAD kinase, antibacterial compound, staphylococci, MRSA



Methods for rapid design and synthesis of new antimicrobial compounds are eagerly sought to battle pathogens and cure infectious diseases.¹ Despite a vast repertoire of methods, quicker routes are still necessary to keep pace with the fast emergence of antibiotic resistance in pathogens. Similarly, the failure of major antibiotic classes calls for rapid identification of novel targets to produce the next generation of anti-infectious agents. NAD kinases (NADKs) have a central role in oxido-reductive functions but are still lacking a quality inhibitor although their important biochemical activity has been known for decades.² The genes encoding the NADKs were discovered by genomic analysis two decades ago,³ and they were shown to be essential for growth in many bacterial species.^{4–6} Interestingly, NADKs belong to a small and particular superfamily of kinases very distantly related to any other NAD or ATP binding proteins.⁷ Indeed, they harbor a two-domain organization made of small alpha/beta fold and an all-beta domain, distantly related only to two lipid kinases existing in humans.⁷ Not only is the fold unique, but also the particular conformation of the NAD in their binding site brings the two ribose moieties in close proximity (distance: ~ 4 Å). This distance is much longer (~ 7 Å) in other NAD(P) binding sites.⁸ This suggested that NADKs represent promising targets and that specific inhibitors could be designed.

Fragment-based drug design (FBDD) is an attractive method for the rapid discovery of starting points to design new lead compounds. It relies on screening very small molecules, usually with millimolar affinity. Their small size allows an exhaustive diverse search with a few molecules (10^2 to 10^4 molecules) within the corresponding chemical space (an estimated 10^7 molecules).⁹ This rational approach has already produced new ligands with affinities in the nanomolar range for several targets,¹⁰ and yielded three clinical drugs. However, fragment optimization to build higher affinity binders, and particularly fragment linking, is still not straightforward,¹⁰ despite the seminal discovery of high affinity inhibitors of the FK506 binding protein and additional attempts since then.^{11–13} In theory,¹⁴ perfect linking of two or three fragments with an expected low millimolar affinity for a target should provide new compounds with low micromolar or nanomolar activity and hence a rapid route toward a promising lead compound, but this is rarely achieved. Currently, there is no single method to efficiently guide the connection of selected fragments, which requires both affinity estimates and

Received: September 25, 2019

Published: February 4, 2020

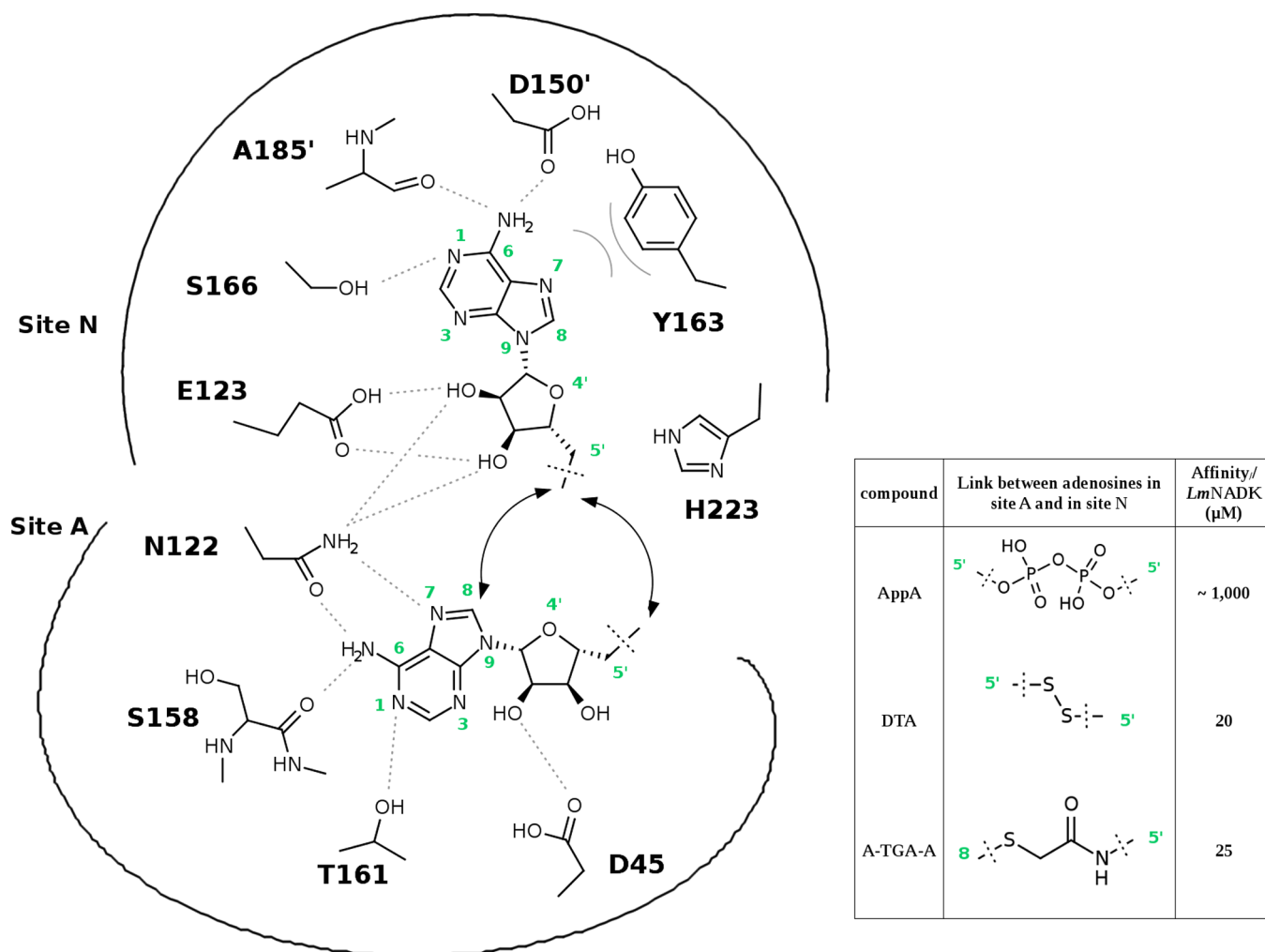


Figure 1. Mapping the binding site to design a library: schematic structure of *LmNADK1* binding site with known diadenosine inhibitors. Adenosine moieties are linked by a pyrophosphate group (AppA), a disulfide bridge (DTA),¹³ or a C8–N5' thio glycolic acid (A-TGA-A).¹⁵ Corresponding affinities for *LmNADK* are shown in the table in the right corner.

66 accurate geometric information. Indeed, FBDD relies on
 67 several techniques to evaluate binding, either by affinity
 68 measurement (high-concentration assay, microcalorimetry), by
 69 structural analysis (X-ray crystallography), or by NMR, which
 70 can provide affinity measurement and low resolution structural
 71 information but at the expense of large material quantities.
 72 Only X-ray diffraction can routinely provide the atomic
 73 resolution required to guide precise fragment linking. We
 74 imagined using the binary information (binding/not binding)
 75 from X-ray crystallography to derive an approximation of
 76 ligand affinity. This involves screening, at a given concentration
 77 slightly above the expected affinity, chemical compounds that
 78 are closely related to each other (and possibly to the first hits).
 79 They are more likely to bind and also to share important
 80 properties such as solubility to limit potential artifacts. The
 81 chemical modifications of a starting fragment with small
 82 substitutions or atomic variations are often easier than
 83 fragment linking itself, and only a very small amount is
 84 necessary for screening by X-ray crystallography. Thus, binding
 85 events can precisely pinpoint small differences that are
 86 favorable and allow binding site mapping. Optimal substituents
 87 should be easily identified, among which some may nicely
 88 overlay with atoms from the second fragment or one of its own

derivatives. This overlay would provide efficient connectors 89
 between these two fragments. 90

Here, we used a deconstruction approach to synthesize 91
 chemical compounds inhibiting bacterial NADK, a novel 92
 therapeutic target. Its substrate, NAD, shows an affinity in the 93
 millimolar range; hence, an inhibitor in low micromolar range 94
 should be sufficient to dramatically impact its enzymatic 95
 activity. Interestingly, NAD can be mimicked by a symmetrical 96
 diadenosine diphosphate¹⁵ (AppA, Figure 1). In addition, 97
 single adenosines were previously shown to share low 98
 affinity,^{16,17} in the low millimolar range, while occupying the 99
 two subpockets of the active site, named A and N for adenine 100
 and nicotinamide (Figure 1). 101

We also showed that the ribose in the subsite A has limited 102
 interactions with the protein except for one hydrogen bond. 103
 Accordingly, we screened adenine derivatives, instead of 104
 adenosines, in order to find new connectors between the two 105
 subsites. This led us to design a new 3-atom linker that 106
 efficiently connects two adenosines, yielding a compound with 107
 low micromolar inhibition of Gram-positive bacterial NADK. 108
 Importantly, we identified this compound, hereafter NKI1, as 109
 an inhibitor of *S. aureus* infection. 110

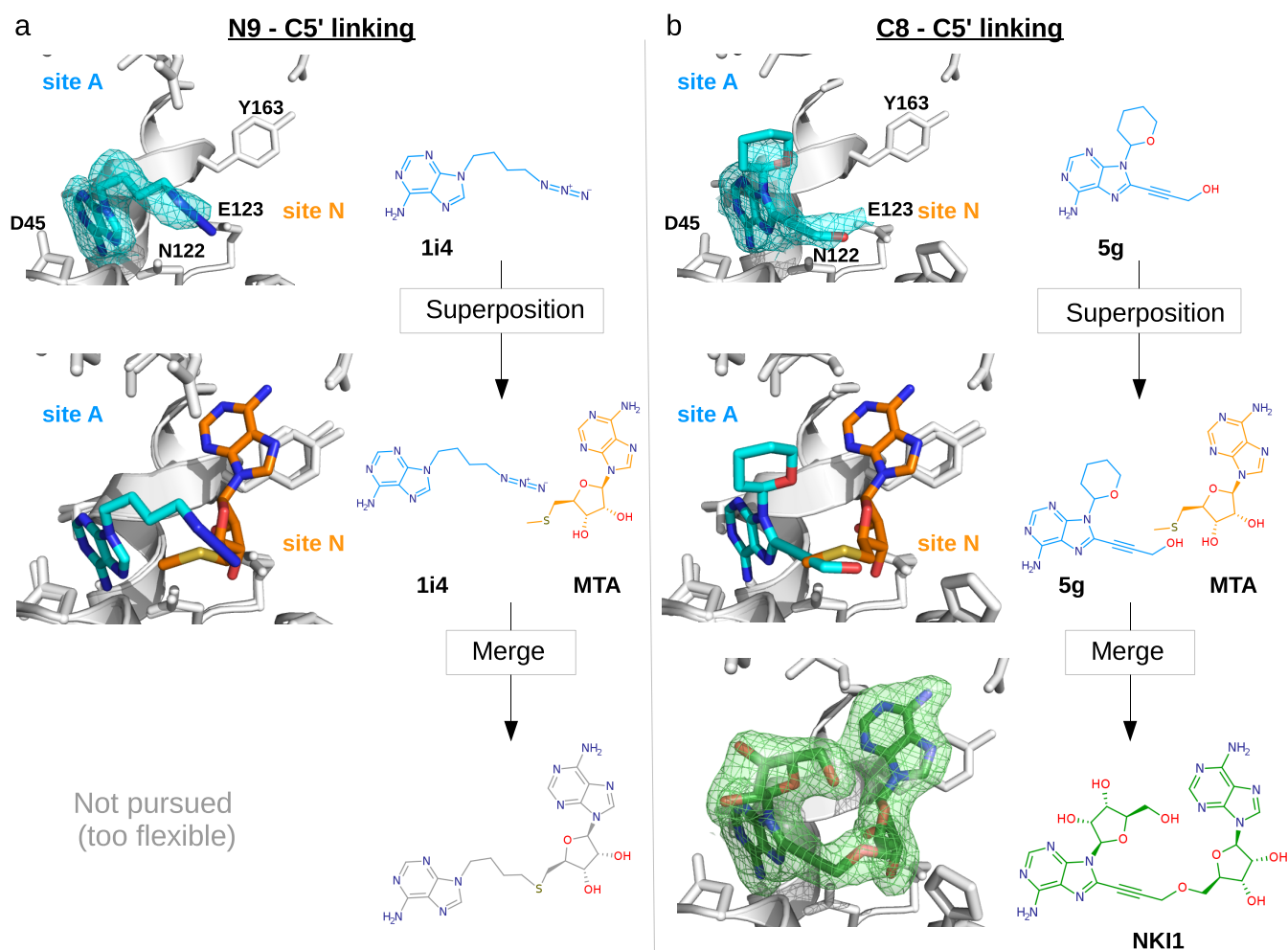


Figure 2. *In crystallo* screening and fragment linking strategy. Two fragment hits bound into the subsite A were used to guide two ways for their linking with an adenosine potentially occupying the subsite N. Linking through position N9 and C5' or through positions C8 and C5' is described in panel (a) and (b), respectively. Crystal structures of two N9 and C8 adenine derivatives (1i4 and 5g, respectively) bound to *LmNADK1* active site are shown in blue. After superimpositions with crystal structures of *LmNADK1* bound to MTA are also shown (MTA in orange). Finally, the crystal structure of our lead compound NK11 bound to *LmNADK1* active site. Views of the $2F_o - F_c$ electron density map in the active site with the ligand molecule omitted in the Fourier synthesis. Map is contoured at 1.0 σ . The picture was generated by the program PYMOL (<http://pymol.sourceforge.net>).

111 ■ RESULTS

112 **Focused Library Design.** We designed a focused library to
 113 map the NAD binding site with X-ray crystallography. A
 114 former screening campaign demonstrated that various
 115 adenosines bearing 5' substitutions can bind into the active
 116 site of the *Listeria monocytogenes* NADK1 (*LmNADK1*) which
 117 is used as a representative enzyme from Gram-positive
 118 bacteria.^{15–17} This screening allowed the exploration of the
 119 binding site in the vicinity of the adenosine 5' ends, which
 120 point toward each other over short distances, as evidenced
 121 previously by the 5'-5' disulfide bridge formed in DTA¹⁵
 122 (Figure 1). It also indicated the rather short N9–N9 or O4'–
 123 O4' distances (6.5 and 5.0 Å, respectively) and an even shorter
 124 one between the C8 position of the adenosine in subsite A and
 125 the 5'-end of the second adenosine in subsite N. Indeed, the 5'
 126 substituent from subsite N points its thiomethyl group toward
 127 the C8 position of the facing adenine at a short distance (S5'–
 128 C8:4.1 Å). Importantly, these features are specific for NADKs
 129 as the vast majority of NAD(P) binding proteins recognize an
 130 elongated conformation of their cofactor.⁸

We wondered whether fragments based on the adenine
 scaffold could fit and provide a better starting point for drug
 design or precise tools to map this active site. Furthermore, we
 considered adenine as an attractive starting point since it can
 be directly derived from functional annotation for ATP- or
 NAD-binding proteins or any other adenine/adenosine
 derivative binding protein. Using a common substructure,
 here the adenine, allows quicker and clearer comparisons of the
 impact of various substituents on binding and easier general-
 ization to other targets.

The crystal structure of the wild-type enzyme bound to its
 substrate or its product highlighted numerous tight contacts
 with the N1, N6, and N7 of adenine (Figure 1). In contrast,
 the N3, C8, and N9 were rather solvent-exposed in both
 subsites. Therefore, positions N3, N9, and C8 could be used to
 build a new link. Since the N3 position was less amenable to
 derivatization, we designed a small focused library of adenine
 bearing substituents at N9 and/or C8 positions.

Screening N9-Derivatives of Adenine by Cocrystallization with *LmNADK1*. The first adenine derivatives of our
 focused library included modifications at the N9 position with

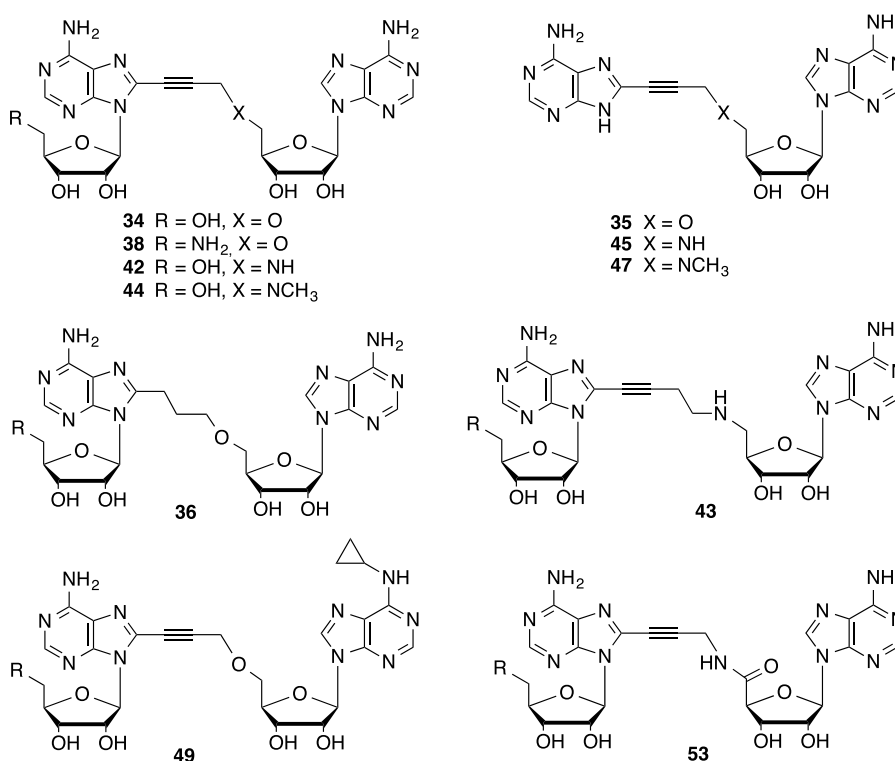


Figure 3. Chemical structures of diadenosine derivatives used in this study.

152 various short and linear alkyl chains bearing 1, 2, 3, or 4
 153 carbons. They were prepared following classical synthetic
 154 routes (Scheme S1). The screening by X-ray crystallography of
 155 20 N9-alkylated adenines (Figure S1) at a final concentration
 156 of 10 mM led to only four complexes with *Lm*NADK1 (Figure
 157 S2). Most soaking and/or cocrystallization led to an empty
 158 crystal structure, suggesting low affinities (>10 mM). No
 159 density was observed for any of the small N9-alkyl chains
 160 irrespective of the terminal group, either polar, e.g., hydroxyl,
 161 thioacetyl, amino, azido, or hydrophobic, e.g., alkynyl (Figure
 162 S1). This suggests that these small substituents fail to provide
 163 favorable interactions in the A or N subsite. Four N9-
 164 derivatives (Figure S2) could be detected in our screen, and
 165 they generally harbored a 4-carbon-long chain, as did the 9-(4-
 166 azidobutyl)-adenine (compound **1i4**, Figure S2a). However,
 167 these N9 substitutions were relatively mobile, again with little
 168 or no favorable interaction with the protein. Nevertheless the
 169 4-azidobutyl extension of compound **1i4** superimposed quite
 170 well with the 5' end of an adenosine in subsite N (Figure 2a).
 171 This path was not pursued further, as the link would be too
 172 flexible to yield a high-affinity compound.

173 The rather limited success of this focused screening of
 174 adenines substituted in N9 only led us to re-evaluate the same
 175 substitutions on an adenine harboring, in addition, a bromo
 176 substituent at the C8 position. The additional bromine atom at
 177 the C8 position was selected to improve the hit-rate, since
 178 brominated adenosine previously showed a gain in affinity in
 179 the adenosine series.^{16,17} Bromination was performed
 180 straightforwardly, and 10 out of 11 compounds were detected
 181 bound into the subsite A (Figure S3), but their pending arms
 182 revealed no particular hot-spot for interactions on the path to
 183 the N subsite (Figure S4). Because these substituted adenines
 184 only occupy the subsite A, they represent a starting point to
 185 grow a fragment from subsite A into a larger compound

occupying the whole active site. On the contrary, the subsite N
 186 remained empty for all the adenines tested. The tilted side
 187 chain of tyrosine Y163 may limit nucleobase entrance in this
 188 subsite, a hindrance counterbalanced by the presence of a
 189 ribose moiety in adenosine derivatives. Accordingly, a
 190 compound made of two adenines linked by their respective
 191 N9 position would not be optimal. Thus, the privileged
 192 fragment for subsite N remained adenosine.^{15–17} However, the
 193 first round of screening highlighted no valuable path from the
 194 N9 position of an adenine placed in the subsite A toward a
 195 facing 5'-end from an adenosine placed in the subsite N. In
 196 order to find a more suitable link toward the subsite N, we
 197 turned to characterize substituted adenines at position C8 that
 198 would be compatible with binding into the subsite A.
 199

Screening C8-Derivatives of Adenine by Cocrystallization with *Lm*NADK1. Previously, *in situ* bond formation
 200 between two bound adenosines revealed a short C8–C5'
 201 linker, a thioacetamide moiety, able to connect subsites A and
 202 N (A-TGA-A, Figure 1). This link provided the first NADK
 203 inhibitor active on bacterial culture *in vitro*.¹⁶ Thus, we
 204 considered other substitutions at the C8 position of adenine
 205 with the aim of linking an adenine in the subsite A and an
 206 adenosine in subsite N. This substitution could fit in the
 207 narrow and rather hydrophobic groove formed by Leu49 and
 208 Gly46.
 209

210 First, position C8 of adenine was substituted with small alkyl
 211 groups (Figure S5). The key synthetic step involved a ring
 212 closure reaction of 2,4,6-triaminopyrimidine (Scheme S2).
 213 Methyl and ethynyl groups (compounds **14a–d** and **3b**) were
 214 accommodated nicely (Figure S6). On the contrary, a
 215 hydrophobic but flexible ethyl group disfavored binding
 216 (compound **10**, Figure S7). Six other small and flexible
 217 substituents at the C8 position did not show any binding
 218 (Figure S7).
 219

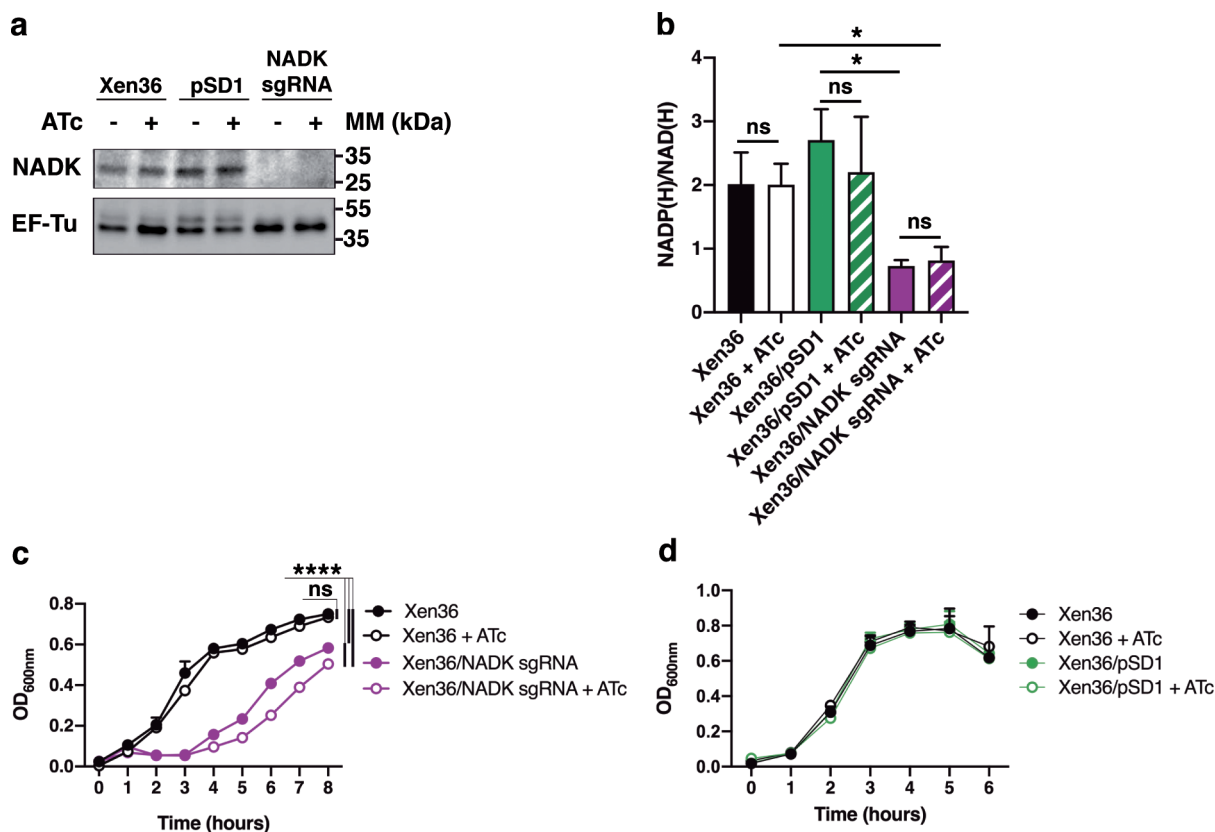


Figure 4. NADK is important for *S. aureus* growth. Bacterial growth was monitored at OD_{600nm} in BHI broth at 37 °C with and without ATc induction. (a) Total bacterial lysates of wild-type (Xen36), control (pSD1), and *ppnK* knock-down (NADK sgRNA) strains were analyzed by immunoblotting using anti-NADK and anti-EF-Tu antibodies. EF-Tu is used as a loading control. The data shown are representative of independent data from two experiments. (b) Levels of NAD(H) and NADP(H) and their ratio were determined by using the NAD/NADH-Glo and NADP/NADPH-Glo assays after growing wild-type (Xen36), control (Xen36/pSD1) and *ppnK* knock-down (Xen36/NADK sgRNA) strains for 6 h ($n = 3$). Bars indicate the standard errors of the means of biological replicates. Comparison of data was performed using a *t* test (ns: nonsignificant, * $p < 0.05$). (c) Growth curves of wild-type (Xen36) and *ppnK* knock-down (Xen36/NADK sgRNA) strains ($n = 6$). Bars indicate the standard errors of the means of biological replicates. Comparison of data was performed using two-way analysis of variance (ns: nonsignificant, **** $p < 0.0001$). (d) Growth curves of wild-type (Xen36) and control (Xen36/pSD1) strains ($n = 6$). Bars indicate the standard errors of the means of biological replicates. Comparison of data was performed using two-way analysis of variance.

220 Then, a 3-hydroxypropynyl group, named hereafter prop-
 221 argyl alcohol, was introduced at position C8 via a Sonogashira
 222 coupling reaction (Figure S8). This substitution led to a clear
 223 electron density in the crystal structure only in the presence of
 224 a cyclic substituent at the N9 position (compound 5g, Figure
 225 S9). This behavior was similar to that in the absence of
 226 substituents in position C8 (compound 1g). Accordingly, the
 227 propargyl moiety could be accommodated, but its polar and
 228 flexible end might partially counterbalance its hydrophobic
 229 interactions with the neighboring Leu49. Nevertheless, this
 230 structure showed that the triple bond of the propargyl group in
 231 position C8 fits perfectly into a narrow hydrophobic groove
 232 that is conserved among all known NAD kinases.

233 Interestingly, the hydroxyl end group of the propargyl
 234 alcohol superimposed well with the position of the sulfur atom
 235 of a methylthioadenosine molecule that would bind into the
 236 subsite N (MTA, Figure 2b). This rather good match (S5'-O
 237 distance: 1.2 Å) suggested a new linker for the connection of
 238 the adenine in subsite A to an adenosine in subsite N, with a
 239 more rigid and more hydrophobic moiety than the formerly
 240 discovered thioglycolate linker.

241 **Propargyl as a New Connector.** These results prompted
 242 us to evaluate propargyl alcohol as a new linker between the
 243 subsites A and N. We synthesized a diadenosine derivative

linked by the propargyl moiety (compound 34, NK11, Figure 244 f3
 3) as well as an adenine linked by the same connector to an 245 f3
 adenosine (compound 35). Both double-headed molecules 246
 were cocrystallized with *Lm*NADK1 and nicely fit into the 247
 whole active site. In both cases one adenosine head occupies 248
 the subsite N, while the subsite A accommodates either the 249
 other adenosine moiety or an adenine moiety (Figure S10). 250

Subsequently the *O*-propargyl linker was replaced by a *N*- 251
 propargyl linker (compound 42) or a *N*-methylpropargyl linker 252
 (compound 44). These new compounds showed little gain in 253
 affinity against *Lm*NADK or against the NADK from *S. aureus*, 254
 another clinically relevant Gram-positive pathogen (Figure 255
 S10), which shares 57% of sequence identity (corresponding to 256
 40 strictly conserved residues among the 50 ones lying within a 257
 distance shorter than 8 Å to NADP) with its listerial 258
 counterpart. Noteworthy, the active concentration of these 259
 novel compounds is 3 orders of magnitude lower than the 260
 millimolar affinity of NAD for these kinases, which suggested a 261
 potential therapeutic window for treatment as an antibiotic. 262
 Their solubility was not improved and their selectivity index 263
 toward the human counterpart was not significantly impacted. 264

Interestingly, in the presence of a ribose in the subsite A, 265
 most crystal structures revealed two hydrogen bonds involving 266
 its 5' hydroxyl group with the oxygen/nitrogen of the 267

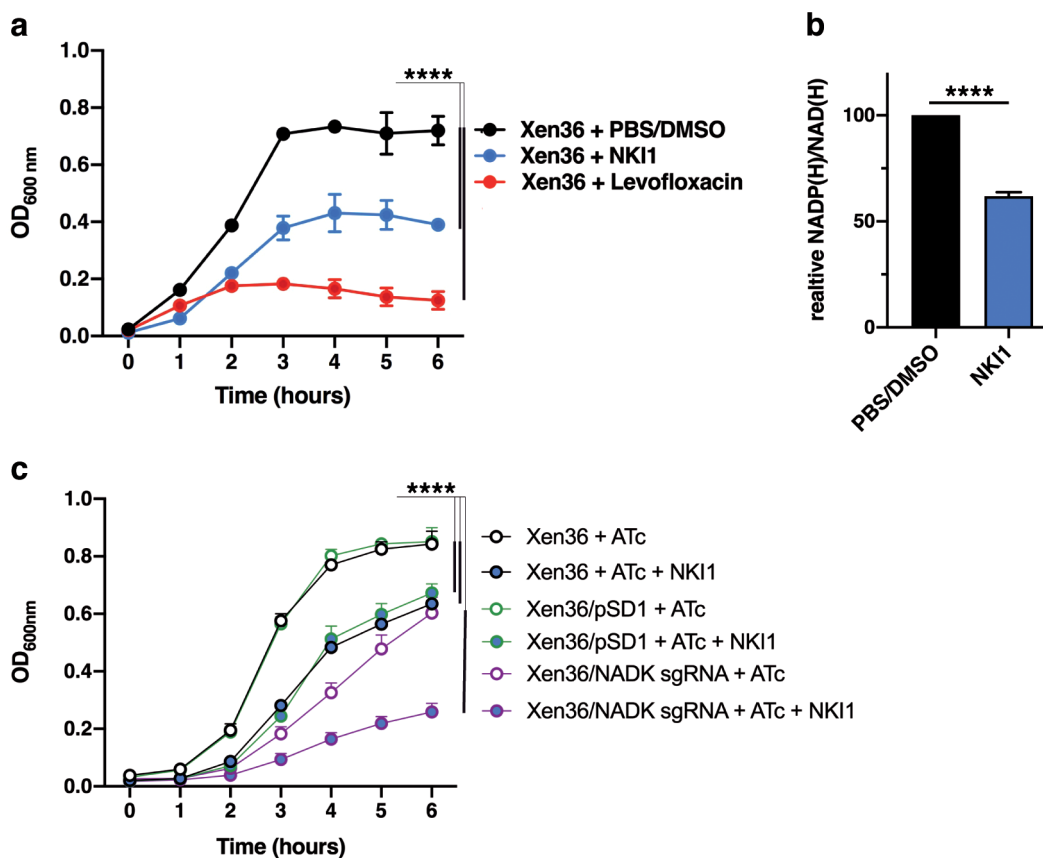


Figure 5. NK11 inhibits *S. aureus* growth *in vitro*. (a) Growth of *S. aureus* Xen36 was monitored at OD_{600nm} in BHI broth at 37 °C. BHI broth was supplemented with PBS/10% DMSO, 0.01 μg/mL NK11 or 10 μg/mL levofloxacin (*n* = 6). Bars indicate the standard errors of the means of biological replicates. Comparison of data was performed using two-way analysis of variance (*****p* < 0.0001). (b) Levels of NAD(H) and NADP(H) and their ratio were determined by using the NAD/NADH-Glo and NADP/NADPH-Glo assays after growing the wild-type Xen36 strain for 6 h in BHI with or without 0.01 μg/mL NK11 (*n* = 3). Bars indicate the standard errors of the means of biological replicates. Comparison of data was performed using a *t* test (*****p* < 0.0001). (c) Growth curves of wild-type (Xen36), control (Xen36/pSD1), and *ppnK* knock-down (Xen36/NADK sgRNA) strains in BHI broth supplemented with ATc, with and without 0.01 μg/mL NK11 (*n* = 6). Bars indicate the standard errors of the means of biological replicates. Comparison of data was performed using two-way analysis of variance (*****p* < 0.0001).

propargyl or the nearby O4' oxygen from the ribose moiety in the subsite N (Figure S10). These internal interactions can stabilize the bound conformation. An attempt to reinforce these interactions with a hydrogen-bond donor failed, as the corresponding 5'-amino group points toward the catalytic aspartate due to a rotation of the ribose (compound 38, Figure S10).

The inhibitory potency of the diadenosine derivatives was tested on recombinant NADKs from *L. monocytogenes* and *S. aureus*. IC₅₀ were determined by measuring formation of reduced NADP produced by the glucose-6-phosphate dehydrogenase coupling enzyme as a readout of NADK activity.^{15–17} Inhibition in the low micromolar range was observed for diadenosine derivatives linked by a *O*- or *N*-(methyl)-propargyl group (compounds 34, 42, 44), while derivatives bearing a flexible three-carbon spacer (*O*-propyl linker, compound 36), an amide group (compound 53) or a four-carbon spacer (compound 43) showed little or no activity against both enzymes (Figure S10).

NADK Is Critical for Growth of *S. aureus*. We next addressed the importance of NADK on *S. aureus* growth *in vitro*. We investigated the impact of decreasing expression of the NADK gene *ppnK* on the growth of *S. aureus* Xen36, a clinical strain. We used the CRISPR interference-based approach described by Zhao and colleagues¹⁸ to knock-down

ppnK. The Xen36 strain was transformed with the *E. coli*/*S. aureus* shuttle plasmid pSD1 or pSD1 containing a single guide RNA (sgRNA) complementary to *ppnK*-specific sequence and the catalytically dead Cas9 (dCas9). Expression of the sgRNA and dCas9 was under the control of the constitutive *S. aureus* promoter P_{flb} and the anhydro-tetracyclin (ATc) inducible promoter P_{tetO}, respectively. Production of NADK by the wild-type, control, and knock-down strains was assessed by immunoblotting. As expected, levels of NADK were strongly reduced in the knock-down strain compared to that of the wild-type and control strains (Figure 4a, Figure S11b). Decreased expression of *ppnK* in the knock-down strain in absence of ATc was presumably due to the known basal activity of the P_{tetO} promoter. We next determined the NADP(H)/NAD(H) ratio in the wild-type, control, and knock-down strains (Figure 4b). The ratio was significantly lower in the knock-down strain than in the wild-type (*p* = 0.03) and control (*p* = 0.01) strains, confirming that the sgRNA targeted *ppnK*. Decreased NADP(H)/NAD(H) ratio in the knock-down strain in absence of ATc corroborated basal activity of the P_{tetO} promoter. Having demonstrated the efficiency of the NADK knock-down, we then measured growth of the wild-type, control, and knock-down strains at OD_{600nm} in BHI with or without ATc. Xen36/NADK sgRNA strain had multiple growth defects in BHI including increased

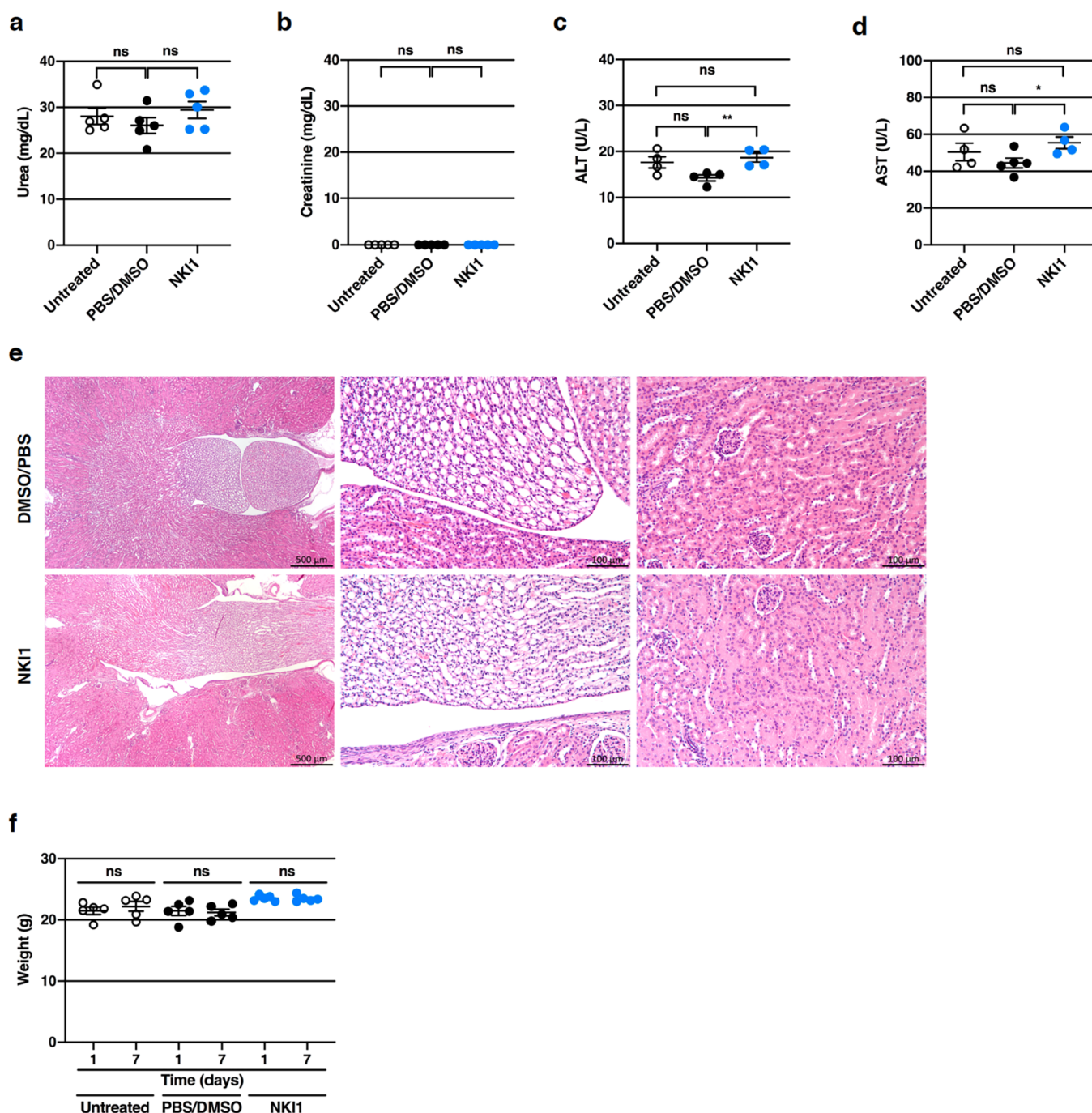


Figure 6. NK11 is not toxic to mice. BALB/c mice were left untreated or treated daily intraperitoneally with PBS/10% DMSO or 2 mg NK11. (a–d) Blood was collected 7 days postinoculation for quantitation of urea (a), creatinine (b), alanine aminotransferase (c), and aspartate aminotransferase (d) using Reflotron strips. Data are means \pm SEM. (e) Histopathological analyses of kidneys of mice 7 days post-treatment. (f) Weight of mice at day 1 and day 7 post-treatment. Data represent mean weights \pm SEM. Comparison of data was performed using a *t* test (ns: nonsignificant, **p* < 0.05, ***p* < 0.01).

318 lag time, decreased doubling time and reduced density in
 319 stationary phase compared to the wild-type strain (Figure 4c).
 320 These defects were even more pronounced when Xen36/
 321 NADK sgRNA was grown in BHI/ATc, while ATc had no
 322 effect on growth of the wild-type strain (Figure 4c and Figure
 323 S11a). Growth defects in the absence of induction
 324 substantiated expression of dCas9 mediated by basal P_{tetO}
 325 activity. In contrast to growth of the knock-down strain,
 326 growth of the pSD1 control strain was similar to that of the

wild-type strain (Figure 4d). Altogether, these results highlight
 the capital role of *ppnK* for *S. aureus* growth.

Given that NADK was critical for *S. aureus* growth, we next
 examined whether diadenosine derivatives could inhibit
 bacterial multiplication *in vitro*. The addition to *S. aureus*
 cultures of a diadenosine linked by a propargyl (compound 34,
 hereafter NK11), strongly affected bacterial growth (Figure
 5a). The lag, log, and plateau phases of NK11 treated bacteria
 were significantly impaired compared to that of bacteria treated
 with the solvent. As expected, growth of bacteria treated with

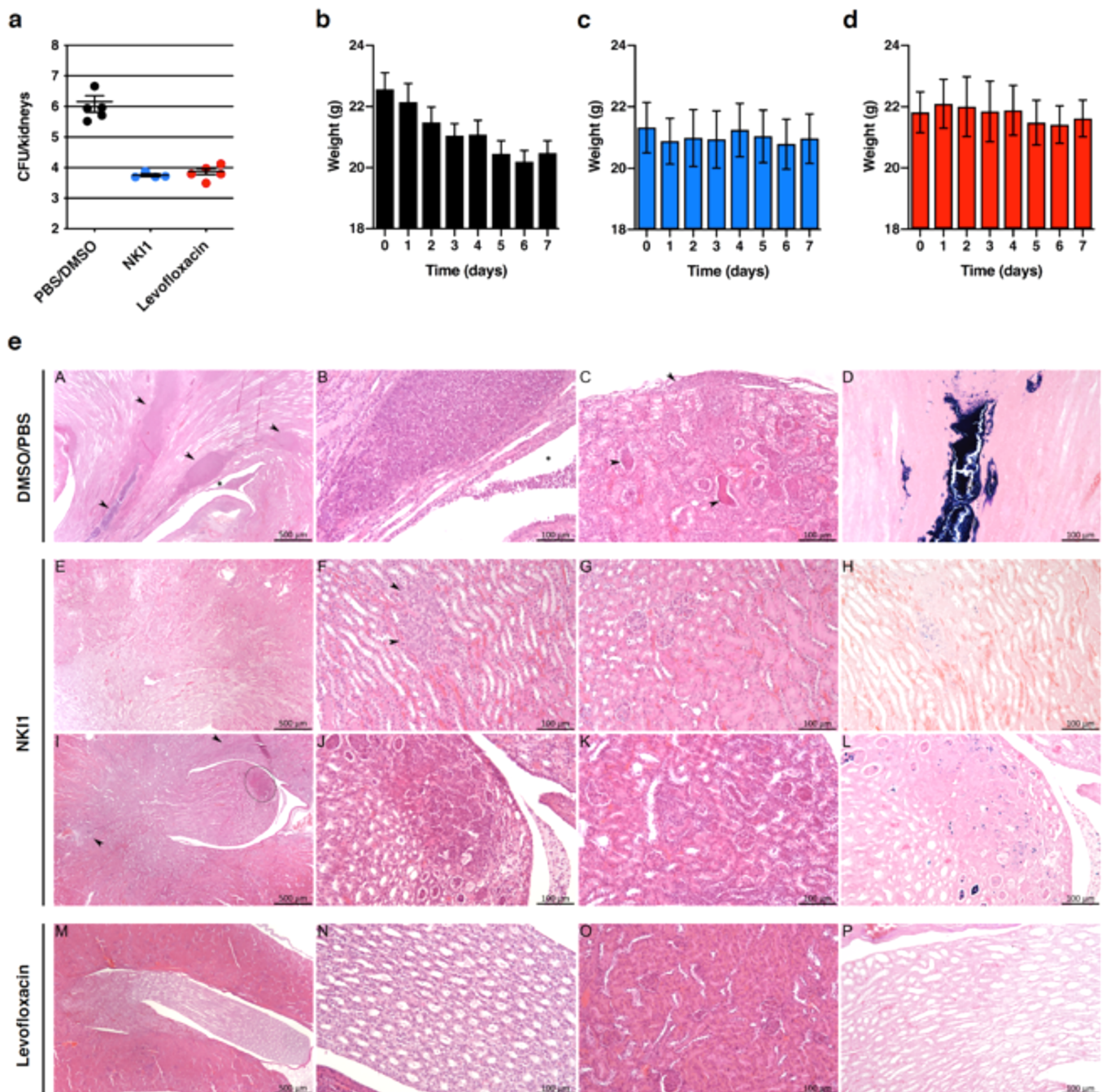


Figure 7. NK11 treatment controls *S. aureus* infection *in vivo*. BALB/c mice were infected intravenously with 5×10^7 *S. aureus* Xen36 and treated daily intraperitoneally with 2 mg NK11 or 2 mg levofloxacin. Control mice received PBS/10% DMSO. (a) Bacterial burden in kidneys of mice 7 days postinfection. Data are mean CFUs in two kidneys \pm SEM. (b–d) Daily weight of infected mice of the control group (b), NK11 group (c), and levofloxacin group (d). The bars represent mean weights \pm SEM. (e) Histopathological analyses of kidneys of mice 7 days postinfection. Representative images of hematoxylin/eosin and/or Gram stained sections from untreated ($n = 8$) or treated mice ($n = 8$). Panels A–D, murine pyelonephritis of the control group (DMSO/PBS). Panel A, ascending inflammation reaching the cortex and necrosis of the papilla. Arrowheads, suppuration. Panel B, infiltration of neutrophils in the renal tubes and interstitium. Panel C, infiltration of neutrophils in the cortex and subcapsular space. Arrowheads, infiltration in the renal tubes. Panel D, Gram-stained bacteria. Panels E–L, lesions of NK11-treated mice. Panels E–G, small cortical inflammatory infiltrates. Arrowheads, inflammatory infiltrates. Panel H, Gram-stained bacteria. Panels I–K, mild pyelonephritis, Panel L, Gram-stained bacteria. Panels M–P, kidney sections of mice treated with levofloxacin. Panels M–O, absence of lesions. Panel P, absence of bacteria.

337 levofloxacin was severely reduced compared to growth of
 338 bacteria in absence of antibiotics. We next determined the
 339 NADP(H)/NAD(H) ratio in bacteria grown in BHI with or
 340 without NK11 (Figure 5b). The ratio was significantly lower in
 341 bacteria treated with NK11, suggesting that NK11 targeted

NADK. To determine if NK11 antibacterial activity was solely
 342 dependent on NADK inhibition, we then measured growth of
 343 the wild-type, control, and knock-down strains at OD_{600nm} in
 344 BHI with ATc, with and without NK11. Growth of the three
 345 strains were significantly impaired by addition of NK11, 346

347 confirming the antibacterial activity of NKI1 and suggesting
348 that other pathways may be affected by NKI1 when its primary
349 target is depleted (Figure 5c). Together, these results indicate
350 that NKI1 inhibits growth of *S. aureus* by targeting NADK and
351 presumably other mechanisms.

352 **NKI1 Is Not Toxic to Human Cells *In Vitro* or to Mice**
353 ***In Vivo***. Because mammals also possess NADKs, we
354 determined the effect of NADK inhibitors on human cell
355 lines. All synthesized diadenosine derivatives, including NKI1,
356 were assayed for cytotoxicity on MRC-5 human fetal lung
357 fibroblasts. The percentage of dead cells after 3 days of
358 incubation with NKI1 was $0 \pm 4\%$ at a concentration of 10^{-5}
359 M and $0 \pm 6\%$ at 10^{-4} M. Therefore, NKI1 acts as an antibiotic
360 without detrimental effects on human cells. Before testing
361 NKI1 toxicity *in vivo*, we assessed the stability of NKI1 by
362 standard liver microsomal and plasma stability assays *in vitro*.
363 We could not detect any significant degradation of NKI1 for 1
364 h at 37 °C in the presence of liver drug metabolizing enzymes
365 (Figure S12a) or plasma hydrolytic enzymes (Figure S12b),
366 pointing to high stability of the compound.

367 To determine the impact of the compound on organ
368 functions, we next analyzed markers of organ failure in plasma
369 from untreated BALB/c mice or from mice treated with NKI1
370 or PBS/DMSO used as the vehicle for NKI1. We found that
371 urea, creatinine, alanine transaminase and aspartate trans-
372 aminase were not increased in mouse plasma upon NKI1
373 treatment nor upon injection of the vehicle alone, consistent
374 with preserved kidney, liver, muscle, and heart functions
375 (Figure 6a–d). Histological analysis confirmed the absence of
376 detectable kidney abnormalities in mice treated with NKI1
377 (Figure 6e). Additionally, treated mice did not show any
378 physical signs of discomfort and did not lose any weight
379 (Figure 6f).

380 **NKI1 Contributes to Bacterial Clearance in *S. aureus***
381 **Infected Mice**. Given that NKI1 has an antibacterial activity
382 against *S. aureus in vitro*, the effect of NKI1 was addressed *in*
383 *vivo*. We evaluated the antibacterial activity of the compound
384 in a murine model of acute hematogenous pyelonephritis
385 induced by the *S. aureus* Xen36 strain. BALB/c mice were
386 infected intravenously with 5×10^7 bacteria and received daily
387 intraperitoneal injections of 100 mg/kg NKI1 or levofloxacin
388 as a control antibiotic for 7 days. A vehicle control group
389 received PBS/DMSO. In the absence of antibiotic treatment,
390 high levels of *S. aureus* were detected in the kidneys 7 days
391 postinfection (Figure 7a). In contrast, daily treatment with
392 NKI1 led to an important decline in the kidney bacterial
393 burden. Levofloxacin treatment led to a similar decrease in
394 bacterial counts. Untreated mice progressively lost weight with
395 time (Figure 7b), while the weight of mice treated with NKI1
396 or levofloxacin remained stable (Figure 7c,d), confirming the
397 efficacy of both antibacterial compounds.

398 We next performed a histologic examination of kidneys
399 removed 7 days postinfection with the *S. aureus* Xen36. The
400 microscopic comparison of kidney sections is shown in Figure
401 7e. Kidneys from untreated mice exhibited marked pyeloneph-
402 ritis with papillary necrosis and infiltration of neutrophils
403 (panel A), extending in the renal tubes and interstitium from
404 the papilla to the cortex (panels A and B) and even to the
405 subcapsular space (panel C). High bacterial loads were
406 detected in kidney lesions (panel D). In contrast, kidneys of
407 mice treated with NKI1 had no lesion or a few small abscesses
408 or inflammatory infiltrates in the cortex (panels E–G) with
409 minimal amount of bacteria (panel H). Pyelonephritis detected

in a few mice was less severe than that observed in untreated
mice (panels I–K) with much lower bacterial loads (panel L).
Besides occasional inflammatory infiltrates in the cortex (data
not shown), kidneys of mice treated with levofloxacin did not
display any lesion (panels M–O) or bacteria (panel P).

As the difficulty of treating antibiotic resistant infections is a
growing concern, we next investigated whether NKI1 could be
active on the MRSA strain Xen31 *in vitro* and in the murine
model of hematogenous pyelonephritis described above.
Growth of Xen31 *in vitro* was strongly affected by NKI1,
although not to the level obtained upon levofloxacin treatment,
which was near total inhibition of growth (Figure S13a).
Efficacies of NKI1 and levofloxacin were then compared *in vivo*
by determining the decrease in the number of bacteria in
kidneys of infected mice. Levofloxacin and NKI1 at 100 mg/kg
daily resulted in decreases of 1.5 and 0.5 log₁₀ CFU/kidney
from control levels, respectively (Figure S13b). Mice treated
with NKI1 or levofloxacin lost weight with time (Figure S13d,
S13e), albeit not to the levels exhibited by untreated mice
(Figure S13c), confirming efficacy of both compounds. The
histologic assessment was in agreement with the weight and
bacterial burden quantification, demonstrating that NKI1 and
levofloxacin were capable of reducing the severity of lesions in
mice infected with the MRSA strain Xen31 (Figure S13f).
Untreated mice displayed pyelonephritis characterized by
necrosis of the papilla and infiltration of neutrophils at the
periphery of necrotic foci, in the cortex and in the pelvic cavity
(Figure 7, panels A–C). Massive amounts of bacteria were
detected in the papillary necrotic area (Figure 7, panel D). In
contrast, pyelonephritis was not detected in mice treated with
NKI1. Kidneys were either free from lesion and bacteria
(Figure 7, panels E–H) or displayed focal abscesses and
bacteria in the cortex (Figure 7, panels I, K, and L) without any
lesion in the papilla (Figure 7, panel J). After levofloxacin
treatment, some mice did not display any lesion or bacteria in
the kidneys (Figure 7, panels M–P), while others exhibited
pyelonephritis (Figure 7, panels Q–T). However, neutrophil
infiltration and bacterial load were reduced compared to those
observed in untreated mice. Taken together, these results
suggest that antibacterial activity of NKI1 is not restricted to
MSSA but extends to drug resistant strains.

DISCUSSION

Discovery and design of new antibacterial compounds is
gaining renewed interest due to the emergence of new threats
from drug-resistant bacteria. NADKs represent attractive drug
targets that have so far been understudied. We hypothesized
that adenine could provide a privileged scaffold onto which
substitution could rapidly answer the question regarding hot-
spots in the region linking the two subsites. Knowledge of *a*
priori binders such as the natural ligands and their fragments or
isosteric analogues may represent alternative entities suitable to
interrogate the possible output of a given screening approach.
Previously, two derivatives of adenosine were linked *in situ*¹⁶
but the resulting compound was suboptimal, showing activity
in the 25–50 μM range, similar to the natural reaction product,
NADP.

In this study, we screened a focused library of adenine
derivatives to identify a new linker. It led to a potent chemical
compound, the best inhibitor described so far for a NADK, and
the first which is active *in vivo*. We targeted *S. aureus* as it is
among the most prominent opportunistic pathogenic bacteria
It belongs to the worrisome ESKAPE group of bacteria

472 (*Enterococcus faecium*, *Staphylococcus aureus*, *Klebsiella pneumo-*
473 *niae*, *Acinetobacter baumannii*, *Pseudomonas aeruginosa*, *Enter-*
474 *obacter* sp.) with a high potential to become antibiotic resistant
475 and difficult to treat. While NADK had been convincingly
476 demonstrated to be essential for the survival of several bacteria
477 including *Escherichia coli*,⁴ *Bacillus subtilis*,⁵ and *Mycobacterium*
478 *tuberculosis*,⁶ it was not clear whether the NADK gene *ppnK*
479 was important for *S. aureus* growth as apparently conflicting
480 results had been published.^{19–23} Our data indicated that the
481 knock-down of NADK has a strongly deleterious effect on
482 *S. aureus* growth, consistent with the importance of the enzyme
483 reported by Bae et al.,²¹ Chaudhuri et al.,²² and Yamachika et
484 al.²³ *S. aureus* has the remarkable capacity to trigger a wide
485 array of infections in susceptible hosts, ranging from skin, soft
486 tissue, bone, joint, kidney, and lung infections to life-
487 threatening bacteremia, endocarditis, sepsis, and toxic shock
488 syndrome.²⁴ Several animal models mimicking human
489 infections have been developed to study *S. aureus* pathoge-
490 nicity and test drug candidates,^{25–28} including the murine
491 model of hematogenous pyelonephritis.^{29,30} We show for the
492 first time that the bactericidal potential of NKI1 translates *in*
493 *vivo* into containment of *S. aureus* induced pyelonephritis,
494 which presumably involves host defense mechanisms. NKI1
495 activity was similar to that of levofloxacin, a member of the
496 fluoroquinolone family of antibiotics guideline-recommended
497 to treat acute pyelonephritis in humans^{31,32} and shown to
498 control pyelonephritis induced by *S. aureus* intravenous
499 inoculation in mice.³⁰ Both compounds were efficient at
500 controlling bacterial multiplication in kidneys. As a result, the
501 number and size of tissular lesions and cellular damages were
502 reduced or abrogated. Treated mice recovered from the
503 infection as shown by the absence of physical signs of disease
504 and weight loss. Interestingly, NKI1 was also active on Xen31,
505 an MRSA strain. While NKI1 activity was similar on Xen31
506 and Xen36 *in vitro*, *in vivo* activity against Xen36 was superior
507 to that against Xen31. Xen36 is derived from the Wright strain
508 isolated from a bacteremic patient (ATCC49525). Xen31 was
509 isolated independently from a patient hospitalized in New York
510 City.³³ Xen31 and Xen36 are thus two clinical isolates that
511 presumably differ in many ways including their sensitivity to
512 methicillin and possibly virulence. These characteristics could
513 account for the different levels of efficacy seen with NKI1 but
514 also with levofloxacin.

515 This example illustrates the potential of biology-driven
516 fragment-based drug design where ligand screening is precisely
517 guided by means of X-ray crystallography. Our study
518 exemplified the successful application of a rational linking
519 strategy to derive a new inhibitor. This also illustrates a
520 possibly useful strategy for general FBDD, where each hit to be
521 linked is rapidly derivatized with variable extensions. Despite
522 the absence of precise monitoring of the affinity toward the
523 target, comparisons of closely related compounds can pinpoint
524 either affinity cliffs when small substituents prevent binding or
525 interaction hot-spots when substituting arms show favorable
526 contacts. This can lead to rapid mapping of the active site. The
527 structural information gained so far suggests further possible
528 improvement of the new inhibitor.

529 ■ CONCLUSION

530 We identified the first bacterial NAD kinase inhibitor, NKI1,
531 active both *in vitro* and *in vivo*. Importantly, NKI1 is active
532 against drug-resistant pathogenic bacteria. On-target activity is
533 currently being investigated in *S. aureus* using proteomic and

genetic approaches, based on drug affinity chromatography 534
coupled to mass spectrometry and modulation of gene 535
expression, respectively. The favorable activity against staph- 536
ylococcal infections and the absence of acute toxicity open the 537
way for further optimization of the lead compound NKI1 538
against various bacterial pathogens. 539

540 ■ METHODS

Expression, Purification, and Activity Assay. His- 541
tagged *LmNADK1* was expressed and purified on cobalt- 542
based IMAC resins (Clontech) as previously published.¹⁶ A 543
similar procedure was followed for the orthologs from *S. aureus*. 544
The NAD kinase activity was determined by measuring the 545
absorbance at 340 nm to follow the formation of reduced 546
NADP produced by a coupling enzyme (Glucose-6-phosphate 547
dehydrogenase from yeast). This enzyme and its substrate 548
were purchased from Sigma-Aldrich. The assay was performed 549
in a 0.5 mL sample of 50 mM Tris-HCl pH7.4, 10 mM MgCl₂, 550
2 mM sodium citrate, 1 mM glucose-6-phosphate at 30 °C 551
using a spectrophotometer Eppendorf ECOM 6122. Half- 552
inhibitory concentrations (IC₅₀) were determined, in the 553
presence of 1 mM NAD and 4 mM ATP (for *LmNADK1*) or 2 554
mM ATP for *S. aureus* NADK. Dixon plots were used to 555
determine *K_i* in the presence of 4 mM ATP and three NAD 556
concentrations (0.2, 0.5, and 1 mM). We also checked that the 557
inhibitors had no effect on the coupling enzymes activity. 558

Chemical Synthesis. The synthesis of adenine derivatives 559
used in this study (see Supporting Information, Figure S1) 560
involved the *N*-9 alkylation of a purine derivative (adenine, 6- 561
chloropurine or 8-methyl-adenine), further conversion of the 562
alkyl alcohol into the corresponding thioacetyl, azido, or amino 563
functional groups. Bromination at the C8 position and 564
subsequent Sonogashira cross-coupling reaction afforded the 565
difunctionalized adenine derivatives (compounds 1–9, Scheme 566
S1). The preparation of C8 alkylated adenine derivatives (9– 567
15, Scheme S2) involved the ring closure of the 4,5,6- 568
triaminopyrimidine in the presence of an acid or amide 569
(classical heating or under MW irradiation), followed by *N*-9 570
alkylation. 571

The synthesis of the diadenosine derivatives (Figure 3) 572
involved Sonogashira cross-coupling reaction of the 8- 573
bromoadenosine derivative 30 or 31 (see Supporting 574
Information) with an appropriate alkyne derivative synthesized 575
as illustrated in Scheme S3. Subsequent deprotection afforded 576
the target compounds (34, 36, 38, 42, 43, 44, 49, 53) in good 577
overall yield. 578

Crystallization. A dedicated crystallization kit (24- 579
conditions) was set up to ensure reproducibility from one 580
protein sample to another. Crystals were grown by mixing 1 μL 581
of the protein solution concentrated at 9 mg/mL and 582
complexed with 5'-deoxy-5'-(methylthio)adenosine (MTA) 583
with an equal volume of crystallization buffer (30 mM sodium 584
bromide, 220 mM potassium citrate, pH 4.8–5.1, glycerol 6%, 585
15–16% w/v polyethylene glycol 400), equilibrated over 0.5 586
mL of the same buffer. As described previously, the complexes 587
with bound ligands were solved using crystals in the 588
orthorhombic form. After growing them in the presence of 589
MTA, crystals were soaked with a 10 mM concentration of the 590
desired ligand in a pre-equilibrated hanging-drop. 591

Crystallographic Studies. X-ray structure determinations 592
were performed using molecular replacement. Refinement was 593
performed using Phenix.³⁴ As in the case of the monoclinic 594
form, some side chains and several short segments of the 595

596 protein (mainly loops 69-TGHL-72, 110-GIGKK-114 and less
597 frequently 129-SGGP-132) were not clearly visible in most
598 electron density maps or showed alternating configurations.
599 Similarly, the last residue and/or the affinity-tag could not be
600 modeled in most protein–ligand complexes. Figures of ligands
601 and corresponding electronic density were generated using
602 PyMOL (<http://pymol.sourceforge.net>). Refinement statistics
603 are provided in Tables S1–S10.

604 **Database Accession Codes.** The refined models and
605 structure factors have been deposited in the Research
606 Collaboratory for Structural Biology (<http://www.rcsb.org>)
607 under the following PDB accession numbers: 6RBO, 6RBP,
608 6RBQ, 6RR2, 6RBR, 6RBS, 6RBT, 6RBU, 6RBV, 6RBW,
609 6RBX, 6RBY, 6RBZ, 6RC0, 6RC1, 6RC2, 6RC3, 6RC4, 6RC5,
610 6RC6, 6RG6, 6RG7, 6RG8, 6RG9, 6RGA, 6RGB, 6RGC,
611 6RGD.

612 **Bacterial Strains and Culture Conditions.** *Staphy-*
613 *lococcus aureus* Xen36 and Xen31 were obtained from Caliper
614 Life Science. Xen36 was derived from a clinical strain isolated
615 from a bacteremic patient (ATCC 49525). Xen31 was derived
616 from a clinical MRSA isolated in Elmhurst Hospital in New
617 York (ATCC 33591). *Staphylococcus aureus* RN4220 is a
618 restriction-deficient laboratory strain widely used for cloning
619 (ATCC 35556). *S. aureus* strains were grown in Brain Heart
620 Infusion (BHI) broth (BD) with shaking at 200 rpm or on
621 BHI agar plates at 37 °C. *Escherichia coli* TOP10 were obtained
622 from Invitrogen and grown in LB broth with shaking at 200
623 rpm or on LB agar plates at 37 °C. When required, culture
624 medium was supplemented with antibiotics (carbenicillin 100
625 µg/mL for *E. coli*, chloramphenicol 15 µg/mL, anhydro-
626 tetracyclin 100 ng/mL for *S. aureus*).

627 **Construction of the *ppnK* Knockdown Plasmid.** The
628 plasmid pSD1 was a gift from Changlong Zhao.¹⁸ The two
629 primers *ppnK*-sgRNA-oligo1 (CTAATTGTTATTTCA-
630 GTTGGTGGTGA) and *ppnK*-sgRNA-oligo2 (AACTC-
631 ACCACCAACTGAAATAACAAT) were used as sgRNA.
632 They were annealed and cloned into *SapI*-digested pSD1,
633 resulting in plasmid pOD134 (*NADK* sgRNA). *E. coli* TOP10
634 was transformed with pOD134, creating strain OD336.

635 **Preparation of Electrocompetent *S. aureus*.** Five
636 milliliters of BHI broth were inoculated with a single colony
637 of *S. aureus* and incubated at 37 °C and 200 rpm overnight.
638 One milliliter of the overnight culture was added to 100 mL of
639 BHI broth and shaken at 200 rpm at 37 °C until an optical
640 density at 600 nm of 0.4 was reached. After 5 min on ice, the
641 culture was centrifuged at 2500g for 10 min at 4 °C. The
642 supernatant was discarded and bacteria were resuspended in 10
643 mL of ice-cold 0.5 M sucrose. Centrifugation and resuspension
644 steps were repeated twice. Bacteria were then resuspended in 1
645 mL of ice-cold 0.5 M sucrose, kept on ice for 15 min, and
646 divided in 100 µL aliquots. Electrocompetent bacteria were
647 stored at –80 °C.

648 **Transformation in *S. aureus*.** Purified pOD134 or pSD1
649 was introduced into *S. aureus* RN4220 and subsequently in
650 *S. aureus* Xen36. Plasmid DNA (200 to 500 ng) and
651 electrocompetent *S. aureus* (100 µL) were mixed and
652 transferred in a 0.2 cm gap-cuvette (Molecular Bioproduct).
653 Strains were transformed by electroporation at 2.5 kV using a
654 Biorad Micro-Pulsar. Immediately after electroporation, 500
655 µL of BHI were added to the cuvette and bacteria were
656 incubated at 37 °C for 1 h with shaking at 200 rpm before
657 plating on BHI agar supplemented with chloramphenicol (7
658 µg/mL). Plates were incubated overnight at 37 °C.

Plasmid Isolation and Purification from *S. aureus*. 659
660 Plasmids were isolated from *S. aureus* using the QIAprep Spin
661 Miniprep Kit (Qiagen) according to the manufacturer's
662 instructions after a cell digestion step with 0.5 mg/mL of
663 linstaphaphine (Sigma-Aldrich) for 30 min at 37 °C.

Bacterial Growth Measurement. Overnight *S. aureus* 664
665 cultures in BHI at 37 °C were diluted 1:100 into BHI broth.
666 For NADK inhibition experiments, culture medium was
667 supplemented with 0 to 100 ng/mL anhydrotetracycline
668 (Sigma-Aldrich) and 25 µg/mL chloramphenicol when
669 required. For antibiotic activity assay, culture medium was
670 supplemented with 25% PBS/10% DMSO, 0.01 µg/mL NKI1
671 in 25% PBS/10% DMSO or 10 µg/mL levofloxacin. Cultures
672 were incubated in 96-well plates or in Erlenmeyer, with shaking
673 at 200 rpm at 37 °C. Growth was monitored with a microplate
674 reader (Glomax Discover, Promega). Experiments were
675 performed at least three times.

Immunoblotting. Bacteria grown for 3 or 6 h were 676
677 collected by centrifugation 10 min at 10 000 rpm at 4 °C and
678 resuspended in 500 µL of PBS. Bacteria were lysed by 6 cycles
679 of 10-s sonication and 10-s rest on ice. Lysates were
680 centrifuged for 15 min at 10 000 rpm at 4 °C and supernatants
681 collected for protein quantification using the Qubit Protein
682 Assay (Invitrogen). Samples were mixed with Laemmli buffer
683 (Biorad) and 10% β-mercaptoethanol and denatured for 5 min
684 at 95 °C. Samples were separated onto 4–20% MiniProtean
685 TGX Stain-Free Precast Gel (Biorad) in TGS buffer and
686 transferred on polyvinylidene fluoride membranes. Membranes
687 were incubated overnight at 4 °C with primary antibodies
688 diluted in 5% blotto (R114 rabbit anti-EF-Tu polyclonal
689 antibodies, 1:5000; R250 rabbit polyclonal anti-*S. aureus*
690 NADK antibodies, 1:1000). Membranes were then incubated
691 with 1:2500 antirabbit horseradish peroxidase-conjugated
692 antibodies (Abcam). Blots were revealed using the ECL kit
693 (Pierce).

NADP(H)/NAD(H) Quantitation. Levels of NAD(H) and 694
695 NADP(H) were assessed by using the NAD/NADH-Glo assay
696 (Promega) and NADP/NADPH-Glo assay (Promega),
697 respectively. Briefly, bacteria were grown 6 h at 37 °C and
698 180 rpm. Growth was stopped by addition of 100 µL of
699 reconstituted detection reagent to 100 µL of bacterial
700 suspension. Samples were incubated for 45 min at room
701 temperature and bioluminescence was measured on a GloMax
702 Discover plate reader. Bioluminescence signal was normalized
703 to OD_{600nm}.

Cytotoxicity Assay. Increasing concentrations of diade- 704
705 nosine derivatives were added to MRC-5 human fetal lung
706 fibroblasts for 3 days and cell viability was assayed using a
707 quantitative metabolic assay with MTT (3-(4,5-dimethylth-
708 iazol-2-yl)-2,5-diphenyltetrazolium bromide) by the Imagif
709 platform (Institut de Chimie des Substances Naturelles Gif-
710 sur-Yvette, France). Measurements were performed in
711 triplicate with a Biomek workstation (Beckman) in 96-well
712 plates.

Metabolic Stability. A microsomal stability assay to 713
714 measure *in vitro* intrinsic clearance and identify putative
715 metabolites formed was performed by the TechMed platform
716 (ESBS, Strasbourg, France). Briefly, 1 µM NKI1 was incubated
717 at 37 °C with human liver microsomes (0.5 mg/mL)
718 containing 1 mM NADPH and 3 mM MgCl₂. Samples were
719 taken every 15 min and enzymatic reactions were stopped by
720 addition of acetonitrile at 0 °C. The percentage of remaining
721 NKI1 was determined by LC-MS/MS by measuring the area

722 under the peak of the compound on the chromatogram.
 723 Testosterone was used as positive control.
 724 **In Vitro Plasma Stability.** Plasma stability was performed
 725 by the TechMed platform (ESBS, Strasbourg, France). Briefly,
 726 1 μ M NK11 was incubated at 37 °C with CD-1 mice plasma
 727 (400 μ L). After 30 min incubation, samples (70 μ L) were
 728 taken every 15 min and reactions were stopped by addition of
 729 acetonitrile (175 μ L) at 0 °C. Samples were then sonicated
 730 and centrifuged for 5 min at 4 °C, and the supernatants
 731 analyzed by LC-MS/MS. The percentage of remaining NK11
 732 was determined by measuring the area under the peak of the
 733 compound on the chromatogram. Parocaine was used as
 734 positive control.
 735 **Mouse Plasma Biochemical Parameters.** Eight-week-
 736 old female BALB/c mice (Charles River) housed under
 737 specific-pathogen-free conditions received food and water ad
 738 libitum. Mice were treated daily intraperitoneally with PBS/
 739 10% DMSO or 2 mg NK11 in PBS/10% DMSO over 7 days.
 740 Mouse weight was monitored every day. Blood was collected
 741 after 7 days of treatment for quantitation of urea, creatinine,
 742 alanine aminotransferase (ALT), and aspartate aminotransfer-
 743 ase (AST) using Reflotron strips (Roche) with Reflovet (Scil).
 744 The kidneys were collected aseptically after 7 days for
 745 histological analysis.
 746 **Mouse Infection Model.** Eight-week-old female BALB/c
 747 mice (Charles River) housed under specific-pathogen-free
 748 conditions received food and water ad libitum and their weight
 749 was recorded every day throughout the duration of the
 750 experiment. Mice were infected intravenously with 5×10^7
 751 bacteria for the Xen36 strain or 10^7 bacteria for the Xen31
 752 strain. Mice were sacrificed 7 days postinfection. Kidneys were
 753 dissected under aseptic conditions for bacteriological and
 754 histological analysis. The number of CFU was determined by
 755 plating serial dilutions of organ homogenates on BHI agar.
 756 **Mouse Histology.** During necropsy, the kidneys were
 757 removed, immediately fixed in 10% neutral-buffered formalin
 758 for 1 week and embedded in paraffin. Transverse 4 μ m-thick
 759 sections were cut for one kidney and longitudinal sections for
 760 the other. For a low number of mice, the papilla was
 761 incompletely or not observed on the longitudinal section
 762 because of the section orientation. Sections were stained in
 763 hematoxylin/eosin. Bacteria were highlighted using Gram
 764 stain.
 765 **Statistical Analysis.** Results are expressed as means \pm
 766 SEM of at least 3 replicates. Statistical analysis was performed
 767 using GraphPad Prism (GraphPad Software). Student's *t*-test
 768 (two-tailed) or two-way ANOVA were used to compare data.
 769 Differences between groups were considered significant when
 770 the *p* value was lower than 0.05.
 771 **Ethical Statement.** All experiments were performed
 772 according to the French national and European laws and
 773 conformed to the European Council Directive on the
 774 approximation of laws, regulations, and administrative
 775 provisions of the Member States regarding the protection of
 776 animals used for experimental and other scientific purposes
 777 (86/609/EEC). The experimental procedures were approved
 778 by the Animal Experiment Committee and the Risk Prevention
 779 Service of the Institut Pasteur (approval numbers 160118 and
 780 18–191).

■ ASSOCIATED CONTENT

781

📄 Supporting Information

782

The Supporting Information is available free of charge at
<https://pubs.acs.org/doi/10.1021/acsinfecdis.9b00368>. 783
 784

Supplementary Figures S1–S13 and Tables S1–S10; 785
 General consideration, experimental procedures for 786
 synthesized library and diadenosine derivatives, includ- 787
 ing Schemes S1–S8, characterization data, and NMR 788
 spectra for compounds used in this study (PDF) 789

■ AUTHOR INFORMATION

790

Corresponding Authors

791

Sylvie Pochet – *Unité de Chimie et Biocatalyse, Institut Pasteur,* 792
CNRS UMR3523, 75015 Paris, France; [orcid.org/0000-](https://orcid.org/0000-0002-7774-7861) 793
0002-7774-7861; Email: sylvie.pochet@pasteur.fr 794

Gilles Labesse – *Centre de Biochimie Structurale, CNRS UMR* 795
5048, INSERM U1054, Université Montpellier, 34090 796
Montpellier, France; Email: labesse@cbs.cnrs.fr 797

Olivier Dussurget – *Unité de Recherche Yersinia, Institut* 798
Pasteur, 75015 Paris, France; Université de Paris, Sorbonne 799
Paris Cité, 75013 Paris, France; Email: [olivier.dussurget@](mailto:olivier.dussurget@pasteur.fr) 800
[pasteur.fr](mailto:olivier.dussurget@pasteur.fr) 801

Authors

802

Muriel Gelin – *Centre de Biochimie Structurale, CNRS UMR* 803
5048, INSERM U1054, Université Montpellier, 34090 804
Montpellier, France 805

Julie Paoletti – *Unité de Chimie et Biocatalyse, Institut Pasteur,* 806
CNRS UMR3523, 75015 Paris, France 807

Marie-Anne Nahori – *Unité des Toxines Bactériennes, Institut* 808
Pasteur, 75015 Paris, France 809

Valérie Huteau – *Unité de Chimie et Biocatalyse, Institut* 810
Pasteur, CNRS UMR3523, 75015 Paris, France 811

Clarisse Leseigneur – *Unité de Recherche Yersinia, Institut* 812
Pasteur, 75015 Paris, France; Université de Paris, Sorbonne 813
Paris Cité, 75013 Paris, France 814

Grégory Jouvion – *Unité de Neuropathologie Expérimentale,* 815
Institut Pasteur, 75015 Paris, France; Sorbonne Université, 816
INSERM UMR S933, Unité de Génétique Médicale, Hôpital 817
Armand Trousseau, 75012 Paris, France 818

Laurence Dugué – *Unité de Chimie et Biocatalyse, Institut* 819
Pasteur, CNRS UMR3523, 75015 Paris, France 820

David Clément – *Unité de Chimie et Biocatalyse, Institut* 821
Pasteur, CNRS UMR3523, 75015 Paris, France; Université de 822
Paris, Sorbonne Paris Cité, 75013 Paris, France 823

Jean-Luc Pons – *Centre de Biochimie Structurale, CNRS UMR* 824
5048, INSERM U1054, Université Montpellier, 34090 825
Montpellier, France 826

Liliane Assairi – *INSERM U759, Institut Curie, Centre* 827
Universitaire Paris Sud, 91405 Orsay, France 828

Complete contact information is available at: 829
<https://pubs.acs.org/10.1021/acsinfecdis.9b00368> 830

Author Contributions

831

[†]M.G., J.P., M.-A.N., and V.H. contributed equally to this 832
 work. M.G. performed crystallography and ligand screening. 833
 M.G. and G.L. refined crystal structures. L.A. performed 834
 protein purification and biochemical studies. J.P., V.H., L.D., 835
 and D.C. performed chemical synthesis. C.L. generated 836
 bacterial strains. M.A.N. and C.L. performed bacterial 837
 experiments *in vitro*. M.A.N., C.L., and O.D. performed *in* 838
vivo experiments. G.J. performed the histological experiments 839

840 and analyzed the data. O.D., S.P., and G.L. coordinated the
841 study, interpreted the data, and wrote the paper.

842 Notes

843 The authors declare no competing financial interest.

844 ■ ACKNOWLEDGMENTS

845 We thank Dr. Changlong Zhao for providing the plasmid
846 pSD1. We wish to acknowledge Dr. Cécile Gasse, Dr. Laurence
847 Morelato, and William Pauly-Batard for their contribution to
848 the preparation of adenine derivatives; Frédéric Bonhomme for
849 assisting with HRMS analysis; the TechMed platform (ESBS,
850 Strasbourg, France) for providing compound stability data; and
851 the Imagif platform (Institut de Chimie des Substances
852 Naturelles, Gif-sur-Yvette, France) for assistance with cytotox-
853 icity assays. We thank Dr. Jean-François Guichou, Dr. Martin
854 Cohen-Gonsaud for helpful discussions and technical help.
855 This work was supported by the Agence Nationale de la
856 Recherche (grants ANR-06-BLAN-0324, ANR-11-EMM-0019,
857 and ANR-17-CE18-0011-02), the Centre National de la
858 Recherche Scientifique (CNRS), Institut National de la
859 Santé et de la Recherche Médicale (INSERM), Institut Pasteur
860 and Institut Curie. DC and CL acknowledge ANR for financial
861 support (ANR-17-CE18-0011-02). We also acknowledge
862 support from the French Infrastructure for Integrated
863 Structural Biology (FRISBI) ANR-10-INSB-05-01 and Idex
864 UP2019. We thank the staff of ESRF and of EMBL-Grenoble
865 for assistance and support in using beamlines ID14-1, ID14-4,
866 ID23-1, ID23-2, ID29, ID30B, ID30A1, and ID30A3.

867 ■ ABBREVIATIONS

868 ATc, anhydro-tetracycline; BHI, brain heart infusion; Cas9,
869 CRISPR associated protein 9; CRISPR, clustered regularly
870 interspaced short palindromic repeats; DMSO, dimethyl
871 sulfoxide; FBDD, fragment-based drug design; LC-MS/MS,
872 liquid chromatography–tandem mass spectrometry; MRSA,
873 methicillin-resistant *Staphylococcus aureus*; NAD, nicotinamide
874 adenine dinucleotide; NADH, reduced form of NAD; NADK,
875 nicotinamide adenine dinucleotide kinase; NADP, nicotina-
876 mide adenine dinucleotide phosphate; NADPH, reduced form
877 of NADP; NK11, NAD kinase inhibitor 1; NMR, nuclear
878 magnetic resonance; OD, optical density; PBS, phosphate
879 buffered saline; sgRNA, single guide RNA.

880 ■ REFERENCES

881 (1) Fischbach, M. A., and Walsh, C. T. (2009) Antibiotics for
882 emerging pathogens. *Science* 325, 1089–1093.
883 (2) McGuinness, E. T., and Butler, J. R. (1985) NAD⁺ kinase—a
884 review. *Int. J. Biochem.* 17, 1–11.
885 (3) Kawai, S., Mori, S., Mukai, T., Suzuki, S., Yamada, T.,
886 Hashimoto, W., and Murata, K. (2000) Inorganic polyphosphate/
887 ATP-NAD kinase of *Micrococcus flavus* and *Mycobacterium tuberculosis*
888 H37Rv. *Biochem. Biophys. Res. Commun.* 276, 57–63.
889 (4) Gerdes, S. Y., Scholle, M. D., D'Souza, M., Bernal, A., Baev, M.,
890 V., Farrell, M., Kurnasov, O. V., Daugherty, M. D., Mseeh, F.,
891 Polanuyer, B. M., Campbell, J. W., Anantha, S., Shatalin, K. Y.,
892 Chowdhury, S. A. K., Fonstein, M. Y., and Osterman, A. L. (2002)
893 From Genetic Footprinting to Antimicrobial Drug Targets: Examples
894 in Cofactor Biosynthetic Pathways. *J. Bacteriol.* 184 (16), 4555–4572.
895 (5) Kobayashi, K., Ehrlich, S. D., Albertini, A., Amati, G., Andersen,
896 K. K., Arnaud, M., Asai, K., Ashikaga, S., Aymerich, S., Bessieres, P.,
897 Boland, F., Brignell, S. C., Bron, S., Bunai, K., Chapuis, J.,
898 Christiansen, L. C., Danchin, A., Débarbouillé, M., Dervyn, E.,
899 Deuerling, E., Devine, K., Devine, S. K., Dreesen, O., Errington, J.,
900 Fillingner, S., Foster, S. J., Fujita, Y., Galizzi, A., Gardan, R., Eschevins,

C., Fukushima, T., Haga, K., Harwood, C. R., Hecker, M., Hosoya, D., 901
Hullo, M. F., Kakeshita, H., Karamata, D., Kasahara, Y., Kawamura, F., 902
Koga, K., Koski, P., Kuwana, R., Imamura, D., Ishimaru, M., Ishikawa, 903
S., Ishio, I., Le Coq, D., Masson, A., Mauël, C., Meima, R., Mellado, R. 904
P., Moir, A., Moriya, S., Nagakawa, E., Nanamiya, H., Nakai, S., 905
Nyggaard, P., Ogura, M., Ohanan, T., O'Reilly, M., O'Rourke, M., 906
Pragai, Z., Pooley, H. M., Rapoport, G., Rawlins, J. P., Rivas, L. A., 907
Rivolta, C., Sadaie, A., Sadaie, Y., Sarvas, M., Sato, T., Saxild, H. H., 908
Scanlan, E., Schumann, W., Seegers, J. F. M. L., Sekiguchi, J., 909
Sekowska, A., Séror, S. J., Simon, M., Stragier, P., Studer, R., 910
Takamatsu, H., Tanaka, T., Takeuchi, M., Thomaidis, H. B., Vagner, 911
V., van Dijl, J. M., Watabe, K., Wipat, A., Yamamoto, H., Yamamoto, 912
M., Yamamoto, Y., Yamane, K., Yata, K., Yoshida, K., Yoshikawa, H., 913
Zuber, U., and Ogasawara, N. (2003) Essential *Bacillus subtilis* genes. 914
Proc. Natl. Acad. Sci. U. S. A. 100, 4678–4683. 915
(6) Sasseti, C. M., Boyd, D. H., and Rubin, E. J. (2003) Genes 916
required for mycobacterial growth defined by high density muta- 917
genesis. *Mol. Microbiol.* 48, 77–84. 918
(7) Labesse, G., Douguet, D., Assairi, L., and Gilles, A. M. (2002) 919
Diacylglyceride kinases, sphingosine kinases and NAD kinases: distant 920
relatives of 6-phosphofructokinases. *Trends Biochem. Sci.* 27, 273–275. 921
(8) Petrelli, R., Sham, Y. Y., Chen, L., Felczak, K., Bennett, E., 922
Wilson, D., Aldrich, C., Yu, J. S., Cappellacci, L., Franchetti, P., 923
Grifantini, M., Mazzola, F., Di Stefano, M., Magni, G., and Pankiewicz, 924
K. W. (2009) Selective inhibition of nicotinamide adenine 925
dinucleotide kinases by dinucleoside disulfide mimics of nicotinamide 926
adenine dinucleotide analogues. *Bioorg. Med. Chem.* 17, S656–S664. 927
(9) Schulz, M. N., and Hubbard, R. E. (2009) Recent progress in 928
fragment-based lead discovery. *Curr. Opin. Pharmacol.* 9, 615–621. 929
(10) Erlanson, D. A., Fesik, S. W., Hubbard, R. E., Jahnke, W., and 930
Jhoti, H. (2016) Twenty years on: the impact of fragments on drug 931
discovery. *Nat. Rev. Drug Discovery* 15, 605–619. 932
(11) Shuker, S. B., Hajduk, P. J., Meadows, R. P., and Fesik, S. W. 933
(1996) Discovering high-affinity ligands for proteins: SAR by NMR. 934
Science 274, 1531–1534. 935
(12) Howard, N., Abell, C., Blakemore, W., Chessari, G., Congreve, 936
M., Howard, S., Jhoti, H., Murray, C. W., Seavers, L. C. A., and van 937
Montfort, R. L. M. (2006) Application of fragment screening and 938
fragment linking to the discovery of novel thrombin inhibitors. *J. Med.* 939
Chem. 49, 1346–1355. 940
(13) Hung, A. W., Silvestre, H. L., Wen, S., Ciulli, A., Blundell, T. L., 941
and Abell, C. (2009) Application of fragment growing and fragment 942
linking to the discovery of inhibitors of *Mycobacterium tuberculosis* 943
pantothenate synthetase. *Angew. Chem., Int. Ed.* 48, 8452–8456. 944
(14) Jencks, W. P. (1981) On the attribution and additivity of 945
binding energies. *Proc. Natl. Acad. Sci. U. S. A.* 78, 4046–4050. 946
(15) Poncet-Montange, G., Assairi, L., Arold, S., Pochet, S., and 947
Labesse, G. (2007) NAD kinases use substrate-assisted catalysis for 948
specific recognition of NAD. *J. Biol. Chem.* 282, 33925–34. 949
(16) Gelin, M., Poncet-Montange, G., Assairi, L., Morelato, L., 950
Huteau, V., Dugué, L., Dussurget, O., Pochet, S., and Labesse, G. 951
(2012) Screening and *in situ* synthesis using crystals of a NAD kinase 952
lead to a potent antistaphylococcal compound. *Structure* 20, 1107– 953
1117. 954
(17) Paoletti, J., Assairi, L., Gelin, M., Huteau, V., Nahori, M. A., 955
Dussurget, O., Labesse, G., and Pochet, S. (2016) 8-Thioalkyl- 956
adenosine derivatives inhibit *Listeria monocytogenes* NAD kinase 957
through a novel binding mode. *Eur. J. Med. Chem.* 124, 1041–1056. 958
(18) Zhao, C., Shu, X., and Sun, B. (2017) Construction of a gene 959
knockdown system based on catalytically inactive ('Dead') Cas9 960
(dCas9) in *Staphylococcus aureus*. *Appl. Environ. Microbiol.* 83, 2026– 961
2015. 962
(19) Ji, Y., Zhang, B., Van, S. F., Horn, Warren, P., Woodnutt, G., 963
Burnham, M. K., and Rosenberg, M. (2001) Identification of critical 964
staphylococcal genes using conditional phenotypes generated by 965
antisense RNA. *Science* 293, 2266–2269. 966
(20) Forsyth, R. A., Haselbeck, R. J., Ohlsen, K. L., Yamamoto, R. T., 967
Xu, H., Trawick, J. D., Wall, D., Wang, L., Brown-Driver, V., Froelich, 968
J. M., C, K. G., King, P., McCarthy, M., Malone, C., Misiner, B., 969

- 970 Robbins, D., Tan, Z., Zhu Zy, Z. Y., Carr, G., Mosca, D. A., Zamudio,
971 C., Foulkes, J. G., and Zyskind, J. W. (2002) A genome-wide strategy
972 for the identification of essential genes in *Staphylococcus aureus*. *Mol.*
973 *Microbiol.* *43*, 1387–1400.
- 974 (21) Bae, T., Banger, A. K., Wallace, A., Glass, E. M., Åslund, F.,
975 Schneewind, O., and Missiakas, D. M. (2004) *Staphylococcus aureus*
976 virulence genes identified by *bursa aurealis* mutagenesis and nematode
977 killing. *Proc. Natl. Acad. Sci. U. S. A.* *101*, 12312–12317.
- 978 (22) Chaudhuri, R. R., Allen, A. G., Owen, P. J., Shalom, G., Stone,
979 K., Harrison, M., Burgis, T. A., Lockyer, M., Garcia-Lara, J., Foster, S.
980 J., Pleasance, S. J., Peters, S. E., Maskell, D. J., and Charles, I. G.
981 (2009) Comprehensive identification of essential *Staphylococcus*
982 *aureus* genes using Transposon-Mediated Differential Hybridisation
983 (TMDH). *BMC Genomics* *10*, 291–218.
- 984 (23) Yamachika, S., Onodera, Y., Hiramatsu, K., and Takase, H.
985 (2012) Plasmid integration method: a new tool for analysis of the
986 essentiality and function of genes in *S. aureus*. *J. Microbiol. Methods* *90*,
987 250–255.
- 988 (24) Lowy, F. D. (1998) *Staphylococcus aureus* infections. *N. Engl. J.*
989 *Med.* *339*, 520–532.
- 990 (25) Tarkowski, A., Collins, L. V., Gjerdtsson, I., Hultgren, O. H.,
991 Jonsson, I.-M., Sakiniene, E., and Verdrengh, M. (2001) Model
992 systems: modeling human staphylococcal arthritis and sepsis in the
993 mouse. *Trends Microbiol.* *9*, 321–326.
- 994 (26) Yu, J., Wu, J., Francis, K. P., Purchio, T. F., and Kadurugamuwa,
995 J. L. (2005) Monitoring *in vivo* fitness of rifampicin-resistant
996 *Staphylococcus aureus* mutants in a mouse biofilm infection model. *J.*
997 *Antimicrob. Chemother.* *55*, 528–534.
- 998 (27) Kugelberg, E., Norstrom, T., Petersen, T. K., Duvold, T.,
999 Andersson, D. I., and Hughes, D. (2005) Establishment of a
1000 superficial skin infection model in mice by using *Staphylococcus*
1001 *aureus* and *Streptococcus pyogenes*. *Antimicrob. Agents Chemother.* *49*,
1002 3435–3441.
- 1003 (28) Kim, H. K., Missiakas, D., and Schneewind, O. (2014) Mouse
1004 models for infectious diseases caused by *Staphylococcus aureus*. *J.*
1005 *Immunol. Methods* *410*, 88–99.
- 1006 (29) Fernandes, P. B., and Swanson, R. N. (1998) Correlation of *in*
1007 *vitro* activities of the fluoroquinolones to their *in vivo* efficacies. *Drugs*
1008 *Exp. Clin. Res.* *14*, 375–378.
- 1009 (30) Froscio, M. B., Melton, J. L., Stewart, F. P., Kulwich, B. A.,
1010 Licata, L., and Barrett, J. F. (1996) *In vivo* efficacies of levofloxacin
1011 and ciprofloxacin in acute murine hematogenous pyelonephritis
1012 induced by methicillin-susceptible and-resistant *Staphylococcus aureus*
1013 strains. *Antimicrob. Agents Chemother.* *40*, 2529–2534.
- 1014 (31) Peterson, J., Kaul, S., Khashab, M., Fisher, A. C., and Kahn, J. B.
1015 (2008) A double-blind, randomized comparison of levofloxacin 750
1016 mg once-daily for five days with ciprofloxacin 400/500 mg twice-daily
1017 for 10 days for the treatment of complicated urinary tract infections
1018 and acute pyelonephritis. *Urology* *71*, 17–22.
- 1019 (32) Noel, G. J. (2009) A review of levofloxacin for the treatment of
1020 bacterial Infections. *Clin. Med.: Therapeutics* *1*, 433–458.
- 1021 (33) Schaefer, S., Perry, W., and Jones, D. (1979) D. Methicillin-
1022 resistant strains of *Staphylococcus aureus* Phage Type 92. *Antimicrob.*
1023 *Agents Chemother.* *15*, 74–80.
- 1024 (34) Adams, P. D., Afonine, P. V., Bunkoczi, G., Chen, V. B., Davis,
1025 I. W., Echols, N., Headd, J. J., Hung, L. W., Kapral, G. J., Grosse-
1026 Kunstleve, R. W., McCoy, A. J., Moriarty, N. W., Oeffner, R., Read, R.
1027 J., Richardson, D. C., Richardson, J. S., Terwilliger, T. C., and Zwart,
1028 P. H. (2010) PHENIX: a comprehensive Python-based system for
1029 macromolecular structure solution. *Acta Crystallogr., Sect. D: Biol.*
1030 *Crystallogr.* *66*, 213–221.